# Production and crystallization of a panel of structure-based mutants of the human myelin peripheral membrane protein P2

**Mari Lehtimäki,[a] Saara Laulumaa,[a,b] Salla Ruskamo[a] and Petri Kursula[a,b,c]***

[a]Department of Biochemistry and Biocenter Oulu, Universtity of Oulu, PO Box 3000, 90014 Oulu, Finland, [b]CSSB–HZI, DESY, Notkestrasse 85, 22603 Hamburg, Germany, and [c]Department of Chemistry, University of Hamburg, Hamburg, Germany

Correspondence e-mail: petri.kursula@oulu.fi

The myelin sheath is a multilayered membrane that surrounds and insulates axons in the nervous system. One of the proteins specific to the peripheral nerve myelin is P2, a protein that is able to stack lipid bilayers. With the goal of obtaining detailed information on the structure–function relationship of P2, 14 structure-based mutated variants of human P2 were generated and produced. The mutants were designed to potentially affect the binding of lipid bilayers by P2. All mutated variants were also crystallized and preliminary crystallographic data are presented. The structural data from the mutants will be combined with diverse functional assays in order to elucidate the fine details of P2 function at the molecular level.

## 1. Introduction

The formation of the lipid-rich myelin sheath around axons is crucial to the normal development and function of the vertebrate nervous system. Myelin is a tightly packed membrane multilayer that carries a specific set of proteins that are important for the formation of myelin and for its interactions with the axon (Snipes & Suter, 1995). A number of neurological diseases, both inherited and autoimmune, are related to myelin abnormalities or degeneration. Myelin-specific proteins are centrally implicated in such diseases, which include peripheral neuropathies and multiple sclerosis (Martin *et al.*, 1992; Kerlero de Rosbo *et al.*, 1993; Suter & Scherer, 2003).

One of the myelin-specific proteins in peripheral nerves is P2, a small 15 kDa protein of the fatty-acid binding protein (FABP) family. P2 is localized into specific areas in compact myelin (Trapp *et al.*, 1984) and is a peripheral membrane protein (Sedzik *et al.*, 1985). P2 has been estimated to comprise up to 15% of the total myelin protein (Greenfield *et al.*, 1973), but its function has remained elusive.

Previously, we have determined the crystal structure of recombinant human P2 in complex with bound palmitate (PDB entry 2wut; Majava *et al.*, 2010). We also showed that P2 is able to stack lipid bilayers (Suresh *et al.*, 2010), possibly in synergy with the myelin basic protein, and that it affects lipid-membrane dynamics (Knoll *et al.*, 2010). While the details of P2–membrane interactions are unclear, the crystal structure suggests the involvement of two opposite faces of P2, both with a high positive charge, in binding between two membranes. Owing to the specific properties of P2 as an FABP and in stacking lipid bilayers, we have a further interest in elucidating the molecular details of the interactions of P2 with lipid bilayers. As one step towards this goal, we designed a panel of mutants based on the human wild-type P2 crystal structure that can be used to study P2 structure and function.

## 2. Materials and methods

### 2.1. Mutagenesis and protein production

For mutagenesis, the expression vector for wild-type human P2 (Majava *et al.*, 2010) containing the human P2 full-length cDNA in the pTH-27 vector (Hammarström *et al.*, 2006) was used as a template in the QuikChange protocol (Stratagene). The primers used in the mutagenesis procedure are listed in Table 1. All mutant constructs

**1359**

**Table 1**
Recombinant protein-production information and primers used for human P2 mutagenesis.

| Source organism | *Homo sapiens* |
|---|---|
| Expression vector | pTH-27 |
| Expression host | *E. coli* Rosetta (DE3) |
| Expression protocol | Autoinduction (4 h at 310 K followed by 48 h at 291 K) |
| Primers used for mutagenesis | |
| N2D | 5′-ATTTTCAGGGCATGAGCGACAAATTCCTGGGCACC-3′ |
| K3N | 5′-ATTTTCAGGGCATGAGCAACAATTTCCTGGGCACC-3′ |
| K21Q | 5′-GAACTTTGACGATTACATGCAGGCTCTGGGTGTGGGGGTTAG-3′ |
| L27D | 5′-AAGCTCTGGGTGTGGGGGATGCCACCAGAAAACTGGG-3′ |
| R30Q | 5′-GGGTGTGGGGGTTAGCCACCCAGAAACTGGGAAATTTGGCCA-3′ |
| K31Q | 5′-GTGGGGGTTAGCCACCAGACAGCTGGGAAATTTGGCCAAA-3′ |
| L35S | 5′-AGCCACCAGAAAACTGGGAAATTCGGCCAAACCCAC-3′ |
| P38G | 5′-AACTGGGAAATTTGGCCAAAGGCACTGTGATCATCAGCAAG-3′ |
| K45S | 5′-GCCAAACCCACTGTGATCATCAGCAAGAGCGGAGATATTATAACTA-3′ |
| F57A | 5′-ATATTATAACTATACGAACTGAAAGTACCGCTAAAAATACAGAAATCTCCTTCAAGCTAG-3′ |
| K65Q | 5′-AAAAATACAGAAATCTCCTTCCAGCTAGGCCAGGAATTTGAAG-3′ |
| R88Q | 5′-AAGAGCATCGTAACCCTGCAGCAGGGATCACTGAATCAAGTGCAG-3′ |
| K112Q | 5′-ATAAAGAGAAAGCTAGTGAATGGGCAGATGGTAGCGGAATGTAAAATGAAG-3′ |
| K120S | 5′-AAAATGGTAGCGGAATGTAAAATGAGCGGCGTGGTGTGCA-3′ |

**Table 2**
Crystallization conditions for the crystals used for data collection for the human P2 mutants.

| Mutant | Well solution | Temperature (K) |
|---|---|---|
| N2D | 36% PEG 6000, 0.1 *M* citrate pH 5.5 | 277 |
| K3N | 35% PEG 6000, 0.1 *M* citrate pH 5.0 | 277 |
| K21Q | 38% PEG 6000, 0.1 *M* citrate pH 5.0 | 277 |
| L27D | 38% PEG 6000, 0.1 *M* citrate pH 5.0 | 291 |
| R30Q | 3.6 *M* ammonium sulfate, 10% glycerol | 291 |
| K31Q | 32% PEG 6000, 0.1 *M* citrate pH 5.0 | 277 |
| L35S | 3.6 *M* ammonium sulfate, 0.1 *M* HEPES pH 7.0 | 291 |
| P38G | 40% PEG 1000, 0.1 *M* citrate pH 5.0 | 277 |
| K45S | 45% PEG 550 MME, 0.1 *M* citrate pH 5.0 | 291 |
| F57A | 42% PEG 6000, 0.1 *M* bis-tris pH 6.0 | 277 |
| K65Q | 40% PEG 1000, 0.1 *M* citrate pH 4.5 | 291 |
| R88Q | 40% PEG 1000, 0.1 *M* citrate pH 5.0 | 291 |
| K112Q | 3.2 *M* ammonium sulfate, 10% glycerol | 291 |
| K120S | 30% PEG 6000, 0.1 *M* citrate pH 5.0 | 277 |

induction (Studier, 2005); after purification of the affinity-tagged protein on Ni–NTA, the His tag was cleaved using TEV protease (van den Berg *et al.*, 2006). After cleavage of the tag, one extra glycine residue remained at the N-terminus of the recombinant P2 before the starting methionine. The final purification step consisted of size-exclusion chromatography and concentration in 20 m*M* HEPES pH 7.5, 150 m*M* NaCl, 10% glycerol.

were sequenced to confirm the presence of the desired mutation. Protein expression and purification (Table 1) were carried out exactly as previously described for the wild-type protein (Majava *et al.*, 2010). Briefly, expression was performed in *Escherichia coli* using auto-

## 2.2. Crystallization

All of the human P2 mutants were crystallized by sitting-drop vapour diffusion on MRC crystallization plates (Molecular Dimensions). The protein concentration for crystallization was approximately 5 mg ml⁻¹; drops consisting of 0.5 µl protein solution and 0.5 µl well solution were equilibrated against 50 µl well solution. Crystallization experiments were carried out in parallel at 291 and 277 K. The optimized crystallization conditions for each mutant are listed in Table 2.
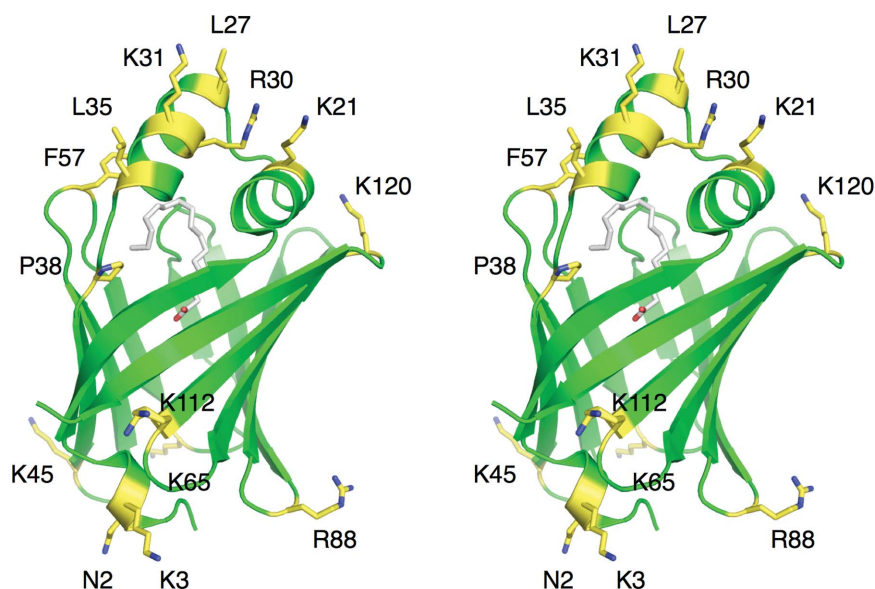


**Figure 1**
Stereoview of the locations of the mutated residues in the human wild-type P2 crystal structure (PDB entry 2wut; Majava *et al.*, 2010). The bound palmitate molecule inside P2 is shown in white. The mutated residues are highlighted in yellow and labelled. The predicted membrane-binding surfaces are at the top and bottom in this view.

**Table 3**
Data collection and processing.

Values in parentheses are for the outer shell.

| Mutant | N2D | K3N | K21Q | L27D | R30Q | K31Q | L35S |
|---|---|---|---|---|---|---|---|
| Wavelength (Å) | 0.97 | 0.91 | 0.97 | 0.97 | 1.0 | 0.91 | 1.0 |
| Crystal-to-detector distance (mm) | 200 | 250 | 250 | 270 | 300 | 200 | 210 |
| Rotation range per image (°) | 0.5 | 0.5 | 0.5 | 0.4 | 1.0 | 0.3 | 0.5 |
| Total rotation range (°) | 90 | 140 | 90 | 120 | 150 | 120 | 160 |
| Exposure time per image (s) | 20 | 30 | 30 | 60 | 60 | 10 | 20 |
| Space group | $P4_12_12$ | $P4_12_12$ | $P4_12_12$ | $P4_12_12$ | $P2_12_12_1$ | $P4_12_12$ | $P4_12_12$ |
| Unit-cell parameters | | | | | | | |
| $\quad a$ (Å) | 58.3 | 64.5 | 58.0 | 64.9 | 58.6 | 58.2 | 65.8 |
| $\quad b$ (Å) | 58.3 | 64.5 | 58.0 | 64.9 | 76.0 | 58.2 | 65.8 |
| $\quad c$ (Å) | 101.7 | 101.2 | 101.2 | 100.9 | 100.6 | 102.2 | 101.3 |
| $\quad \alpha = \gamma$ (°) | 90 | 90 | 90 | 90 | 90 | 90 | 90 |
| $\quad \beta$ | 90 | 90 | 90 | 90 | 90 | 90 | 90 |
| Resolution range (Å) | 30–1.65 (1.70–1.65) | 20–2.70 (2.77–2.70) | 30–2.30 (2.36–2.30) | 30–2.81 (2.88–2.81) | 20–3.00 (3.08–3.00) | 20–1.80 (1.85–1.80) | 20–2.00 (2.05–2.00) |
| Total No. of reflections | 99921 | 67814 | 41115 | 46757 | 43544 | 159455 | 191753 |
| No. of unique reflections | 21068 | 6311 | 8082 | 5609 | 9332 | 16817 | 15619 |
| Completeness† (%) | 97.4 (78.9) | 99.5 (100) | 99.2 (97.6) | 98.8 (98.0) | 98.4 (95.5) | 98.7 (99.8) | 99.8 (98.2) |
| Multiplicity | 4.7 (2.0) | 10.7 (11.2) | 5.1 (4.7) | 8.3 (7.9) | 4.7 (4.6) | 9.5 (9.2) | 12.3 (9.7) |
| $\langle I/\sigma(I)\rangle$ | 15.2 (1.5) | 14.5 (3.1) | 11.1 (2.2) | 12.7 (3.4) | 9.0 (1.2) | 19.0 (2.5) | 19.8 (1.7) |
| $R_{meas}$‡ | 0.090 (0.703) | 0.181 (0.838) | 0.153 (0.846) | 0.156 (0.717) | 0.142 (1.885) | 0.117 (0.981) | 0.104 (1.574) |
| $CC_{1/2}$§ (%) | 99.8 (62.5) | 99.7 (95.0) | 99.5 (70.9) | 99.6 (94.7) | 99.7 (47.9) | 99.9 (78.0) | 99.9 (84.8) |
| Overall $B$ factor from Wilson plot (Å²) | 19 | 37 | 32 | 38 | 81 | 22 | 41 |
| Protein monomers per asymmetric unit | 1 | 1 | 1 | 1 | 2 | 1 | 1 |
| Solvent content (%) | 57 | 65 | 57 | 65 | 67 | 57 | 66 |
| *Phaser* $Z$-score¶ | 27 | 45 | 26 | 41 | 28 | 24 | 31 |

| Mutant | P38G | K45S | F57A | K65Q | R88Q | K112Q | K120S |
|---|---|---|---|---|---|---|---|
| Wavelength (Å) | 1.03 | 1.03 | 1.10 | 1.03 | 0.91 | 1.0 | 0.91 |
| Crystal-to-detector distance (mm) | 200 | 250 | 65 | 110/220 | 200 | 180 | 320 |
| Rotation range per image (°) | 0.25 | 0.4 | 0.5 | 0.5/1.0 | 0.25 | 0.5 | 0.5 |
| Total rotation range (°) | 180 | 180 | 180 | 113/120 | 125 | 150 | 115 |
| Exposure time per image (s) | 20 | 30 | 10 | 30/10 | 10 | 20 | 30 |
| Space group | $P2_12_12_1$ | $C2$ | $C2$ | $P4_3$ | $P4_12_12$ | $P4_12_12$ | $P4_12_12$ |
| Unit-cell parameters | | | | | | | |
| $\quad a$ (Å) | 55.5 | 120.1 | 112.8 | 83.0 | 64.9 | 65.7 | 63.7 |
| $\quad b$ (Å) | 65.5 | 63.6 | 36.1 | 83.0 | 64.9 | 65.7 | 63.7 |
| $\quad c$ (Å) | 82.2 | 84.5 | 31.2 | 77.9 | 264.4 | 101.2 | 101.4 |
| $\quad \alpha = \gamma$ (°) | 90 | 90 | 90 | 90 | 90 | 90 | 90 |
| $\quad \beta$ | 90 | 130.1 | 96.9 | 90 | 90 | 90 | 90 |
| Resolution range (Å) | 20–1.80 (1.85–1.80) | 20–2.20 (2.26–2.20) | 20–1.27 (1.30–1.27) | 20–1.20 (1.23–1.20) | 40–1.80 (1.85–1.80) | 25–1.80 (1.85–1.80) | 20–2.90 (2.98–2.90) |
| Total No. of reflections | 142607 | 76070 | 93246 | 787155 | 389891 | 248391 | 35641 |
| No. of unique reflections | 25915 | 22051 | 31894 | 154301 | 53492 | 21102 | 4976 |
| Completeness† (%) | 91.0 (58.4) | 88.2 (49.4) | 96.8 (77.4) | 93.9 (63.3) | 99.4 (96.9) | 99.6 (96.0) | 99.6 (97.4) |
| Multiplicity | 5.5 (3.7) | 3.4 (2.8) | 2.9 (1.8) | 5.1 (2.1) | 7.3 (5.9) | 11.8 (11.2) | 7.2 (7.3) |
| $\langle I/\sigma(I)\rangle$ | 21.8 (2.2) | 11.1 (1.7) | 8.2 (1.2) | 19.6 (1.4) | 19.8 (2.0) | 30.3 (2.1) | 10.5 (1.8) |
| $R_{meas}$‡ | 0.054 (0.664) | 0.092 (0.728) | 0.092 (0.781) | 0.044 (0.785) | 0.085 (0.841) | 0.063 (1.262) | 0.144 (1.445) |
| $CC_{1/2}$§ (%) | 99.9 (77.0) | 99.7 (75.3) | 99.6 (43.5) | 100 (56.2) | 99.9 (67.3) | 100 (83.4) | 99.8 (85.9) |
| Overall $B$ factor from Wilson plot (Å²) | 32 | 43 | 17 | 17 | 27 | 34 | 72 |
| Protein monomers per asymmetric unit | 2 | 3 | 1 | 4 | 3 | 1 | 1 |
| Solvent content (%) | 51 | 55 | 41 | 45 | 60 | 66 | 64 |
| *Phaser* $Z$-score¶ | 29 | 41 | 10 | 47 | 33 | 32 | 32 |

† In cases of low completeness in the highest resolution shell, the cause is usually data collection on a square detector, where data were processed all the way to the corners. ‡ $R_{meas}$, the redundancy-independent $R$ factor (Diederichs & Karplus, 1997), is defined as $\sum_{hkl}\{N(hkl)/[N(hkl)-1]\}^{1/2}\sum_i |I_i(hkl) - \langle I(hkl)\rangle|/\sum_{hkl}\sum_i I_i(hkl)$. § $CC_{1/2}$ is the correlation coefficient between two random half data sets, as described by Karplus & Diederichs (2012). ¶ The shown $Z$-score is that for the *Phaser* translation function upon finding the last monomer in the asymmetric unit.

## 2.3. Data collection and processing

Diffraction data were collected on several occasions, using slightly different wavelengths, on the X12 crystallography beamline of the EMBL Hamburg Outstation at the DORIS storage ring of DESY. Data collection was carried out under a stream of gaseous nitrogen at 100 K. Except for the F57A data set, a Rayonics 225 detector was used; for F57A, the detector used was a MAR CCD 165. Diffraction data were processed using *XDS* (Kabsch, 2010) and *XDSi* (Kursula, 2004) and the data statistics are listed in Table 3. The structures were solved by molecular replacement with *Phaser* (McCoy *et al.*, 2007; Adams *et al.*, 2010) using the crystal structure of wild-type human P2 (PDB entry 2wut; Majava *et al.*, 2010) as a model.

## 3. Results and discussion

Based on the crystal structure of human P2 and its predicted membrane-binding surfaces on opposite faces of the protein (Majava *et al.*, 2010), we generated a panel of 14 point mutants for structure–function studies. The goal is to use these mutants to combine the functional data from various membrane-binding assays with high-resolution structural data. This in turn will elucidate the fine detail of the function of P2 in myelin membrane stacking.

We mutated both basic surface residues as well as hydrophobic residues predicted to enter into the hydrophobic layer upon bilayer binding. The locations of the mutated residues in the wild-type P2 structure are depicted in Fig. 1. All of the generated mutant variants
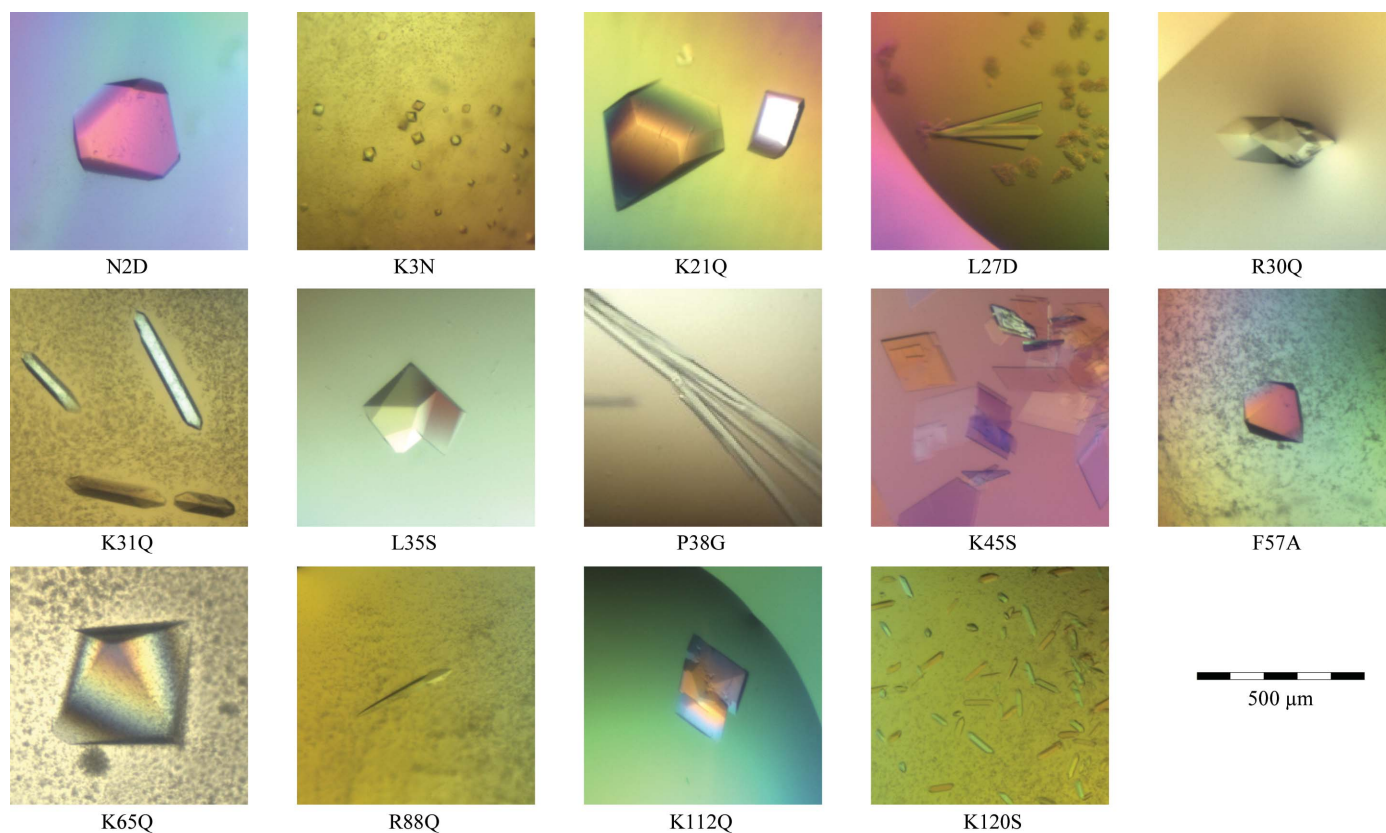
**Figure 2**
Crystals of human P2 mutants. The scale bar at the bottom right applies to all images.

were successfully produced and purified on a large scale and all of them also produced diffraction-quality crystals (Fig. 2, Table 3). Crystals were formed under two basic conditions: high PEG concentrations around pH 5 and high ammonium sulfate concentrations at neutral pH. Despite the limited variability in the crystallization conditions, a number of different crystal forms were observed, which is a sign of different packing induced by the surface mutations.

Interestingly, the best crystals, which were of the K65Q mutant, diffracted X-rays to atomic resolution (1.2 Å), while our previous data from the wild-type protein only extended to 1.8 Å resolution (Majava *et al.*, 2010). The K65Q crystals belonged to the same space group as the wild-type protein, but the *a* and *b* unit-cell dimensions were >10% shorter, indicating much tighter packing. The F57A mutant also diffracted to better than 1.3 Å resolution. Even for those data sets for which $\langle I/\sigma(I)\rangle$ in the highest-resolution shell was below 2, the correlation coefficient between random half data sets (CC$_{1/2}$; Karplus & Diederichs, 2012) indicated significant information content (Table 3). If required in the future, higher resolution data can be collected from some of the mutants.

The structures of all mutants have now been solved by molecular replacement (Table 3) and the crystal structures are currently under refinement and detailed analysis. The mutants are simultaneously being used for functional studies of the human P2 protein both *in vitro* and *in vivo*.

## References

Adams, P. D. *et al.* (2010). *Acta Cryst.* D**66**, 213–221.
Berg, S. van den, Löfdahl, P. A., Härd, T. & Berglund, H. (2006). *J. Biotechnol.* **121**, 291–298.
Diederichs, K. & Karplus, P. A. (1997). *Nature Struct. Biol.* **4**, 269–275.
Greenfield, S., Brostoff, S., Eylar, E. H. & Morell, P. (1973). *J. Neurochem.* **20**, 1207–1216.
Hammarström, M. Woestenenk, E. A., Hellgren, N., Härd, T. & Berglund, H. (2006). *J. Struct. Funct. Genomics*, **7**, 1–14.
Kabsch, W. (2010). *Acta Cryst.* D**66**, 125–132.
Karplus, P. A. & Diederichs, K. (2012). *Science*, **336**, 1030–1033.
Kerlero de Rosbo, N., Milo, R., Lees, M. B., Burger, D., Bernard, C. C. & Ben-Nun, A. (1993). *J. Clin. Invest.* **92**, 2602–2608.
Knoll, W., Natali, F., Peters, J., Nanekar, R., Knoll, W., Wang, C. & Kursula, P. (2010). *Spectroscopy*, **24**, 585–592.
Kursula, P. (2004). *J. Appl. Cryst.* **37**, 347–348.
Majava, V., Polverini, E., Mazzini, A., Nanekar, R., Knoll, W., Peters, J., Natali, F., Baumgärtel, P., Kursula, I. & Kursula, P. (2010). *PLoS One*, **5**, e10300.
Martin, R., McFarland, H. F. & McFarlin, D. E. (1992). *Annu. Rev. Immunol.* **10**, 153–187.
McCoy, A. J., Grosse-Kunstleve, R. W., Adams, P. D., Winn, M. D., Storoni, L. C. & Read, R. J. (2007). *J. Appl. Cryst.* **40**, 658–674.
Sedzik, J., Blaurock, A. E. & Hoechli, M. (1985). *J. Neurochem.* **45**, 844–852.
Snipes, G. J. & Suter, U. (1995). *J. Anat.* **186**, 483–494.
Studier, F. W. (2005). *Protein Expr. Purif.* **41**, 207–234.
Suresh, S., Wang, C., Nanekar, R., Kursula, P. & Edwardson, J. M. (2010). *Biochemistry*, **49**, 3456–3463.
Suter, U. & Scherer, S. S. (2003). *Nature Rev. Neurosci.* **4**, 714–726.
Trapp, B. D., Dubois-Dalcq, M. & Quarles, R. H. (1984). *J. Neurochem.* **43**, 944–948.